

# Strain-Induced Anisotropic Transport Properties of $\text{LaBaCo}_2\text{O}_{5.5+\delta}$ Thin Films on $\text{NdGaO}_3$ Substrates

Ming Liu,<sup>\*,†,‡,§</sup> Qiang Zou,<sup>§,¶</sup> Chunrui Ma,<sup>‡</sup> Greg Collins,<sup>‡</sup> Shao-Bo Mi,<sup>†,||</sup> Chun-Lin Jia,<sup>†,⊥</sup> Haiming Guo,<sup>§</sup> Hongjun Gao,<sup>§</sup> and Chonglin Chen<sup>\*,‡</sup>

<sup>†</sup> Electronic Materials Research Laboratory, Key Laboratory of the Ministry of Education & International Center for Dielectric Research, Xi'an Jiaotong University, Xi'an 710049, People's Republic of China

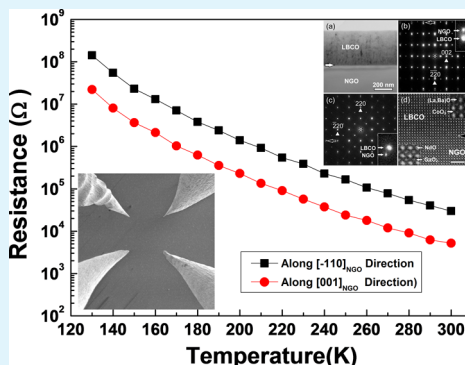
<sup>‡</sup> Department of Physics and Astronomy, University of Texas at San Antonio, San Antonio, Texas 78249, United States

<sup>§</sup> Institute of Physics, Chinese Academy of Sciences, Beijing 100190, People's Republic of China

<sup>||</sup> Shenyang National Laboratory for Materials Science, Institute of Metal Research, Chinese Academy of Sciences, Shenyang 110016, China

<sup>⊥</sup> Peter Grünberg Institute, Forschungszentrum Jülich GmbH, 52425 Jülich, Germany

**ABSTRACT:** Thin films of double-perovskite structural  $\text{LaBaCo}_2\text{O}_{5.5+\delta}$  were epitaxially grown on (110)  $\text{NdGaO}_3$  substrates by pulsed laser deposition. Microstructural studies by high-resolution X-ray diffraction and transmission electron microscopy revealed that the films have an excellent quality epitaxial structure. In addition, strong in-plane anisotropic strains were measured. Electrical transport properties of the films were characterized by an ultra-high-vacuum four-probe scanning tunneling microscopy system at different temperatures. It was found that the anisotropic in-plane strain can significantly tune the values of film resistance up to 590%.



**KEYWORDS:**  $\text{LaBaCo}_2\text{O}_6$  thin film, anisotropic, transport properties, interface

## INTRODUCTION

Complex transition-metal oxides have attracted considerable attention of research due to their electrical, magnetic, and optical properties, which can be used for the development of various new concept devices, such as energy harvest, electrical, and chemical sensors, etc.<sup>1–3</sup> Perovskite cobaltates exhibit remarkable mixed conductivity and catalytic properties at high temperature as well as interesting magnetic and electrical transport properties at low temperature.<sup>4–10</sup> Among them, the oxygen-deficient double perovskite cobaltates  $\text{LnBaCo}_2\text{O}_{5.5+\delta}$  ( $\text{Ln}$  = Lanthanide) show particularly interesting phenomena of the order-disorder at the A-cation sites in the cobaltate system.<sup>11–15</sup> Especially, the very small difference in the A-site cations' radii between  $\text{La}^{3+}$  and  $\text{Ba}^{2+}$  in the  $\text{LaBaCo}_2\text{O}_{5.5+\delta}$  (LBCO) can form complex A-site order, nanoarea order, and disorder layered perovskite structures and induce various exciting physical phenomena, such as various oxidation states ( $\text{Co}^{2+}/\text{Co}^{3+}/\text{Co}^{4+}$ ) of cobalt, different spin state configurations, giant MR effect, metal insulator transition, etc.<sup>16–19</sup> In order to fully understand the magnetic and transport properties of such complex cobalt oxides, the single crystalline samples are critically desired. In our previous work, we have fabricated highly epitaxial single crystalline LBCO thin films on (001)  $\text{LaAlO}_3$ ,<sup>20,21</sup> (001)  $\text{SrTiO}_3$ ,<sup>22,23</sup> and (001)  $\text{MgO}$ <sup>24</sup> and found

that these films possess an extraordinary sensitivity to reducing/oxidizing environments and an exceedingly fast redox reaction at high temperature. Moreover, at low temperatures, the highly epitaxial LBCO thin films exhibit a much larger magnetoresistance value than those from various phases of its bulk material.

Strain engineering has become an important technique in the studies of multifunctional complex oxide thin films and nanoscale materials and has shown significant impact on the microstructures and physical properties of novel-engineered materials.<sup>25,26</sup> In other words, the novel electrical and magnetic properties can be achieved by the strain modification. Normally, the effects of strain on thin films can be studied by choosing the lattice mismatch between films and substrates and controlling the thickness of the films. However, the different level of lattice mismatch will generate different local strain distributions, which will result in the different growth modes and different crystallization qualities and defects densities. Recently, we successfully produced the in-plane anisotropic properties by choosing the (110)  $\text{NdGaO}_3$  (NGO) substrate

Received: March 7, 2014

Accepted: May 13, 2014

Published: May 13, 2014

with different lattice mismatch along two in-plane directions.<sup>27–29</sup> This methodology will also allow the study of the effect of the anisotropic in-plane strain on the properties of highly epitaxial LBCO films on NGO. NGO has an orthorhombic structure with the lattice parameters  $a \sim 0.542$  nm,  $b \sim 0.550$  nm, and  $c \sim 0.771$  nm.<sup>30</sup> On the (110) NGO substrate, the in-plane lattice parameters are  $\sqrt{a^2 + b^2} = 7.733$  along the [110] direction and 7.715 along [001] direction. Considering the lattice parameters (cubic structure  $a = 3.886$  Å) of LBCO, the in-plane strains of 0.5% and 0.7% along the [110] and [001] directions are obtained, respectively. Therefore, in the LBCO/NGO systems, the anisotropic strain effects on the physical properties of the LBCO films can be studied.

## RESULTS AND DISCUSSION

In the present work, the LBCO thin films were grown on (110) NGO by a KrF excimer pulsed laser deposition system with a wavelength of 248 nm. The growth condition was optimized as the energy density of about 2.0 J/cm<sup>2</sup> at 5 Hz, an oxygen pressure of 20 mTorr, and a growth temperature at 800 °C. After the growth, the LBCO films were annealed at 850 °C for 15 min in pure oxygen (200 Torr) and then slowly cooled down to room temperature at the rate of 5 °C/min. The crystallinity and microstructure of the LBCO films were characterized by high-resolution X-ray diffraction (HRXRD) using a PANalytical X'Per MRD and scanning transmission electron microscopy (STEM) using a JEM ARM200F microscope equipped with a probe corrector and operated at 200 kV. The electrical transport properties of the LBCO films were systematically studied using an ultra-high-vacuum four-probe scanning tunneling microscopy (4P-STM) system at different temperatures; the details of the 4P-STM electrical transport measurement have been introduced in our previously published paper.<sup>25,31</sup> Briefly, the square four-terminal method was used for measuring the resistance of thin films. In this method, four probes are placed in a square shape, equally spaced, as shown in Figure 1. Sweeping current is applied on one pair of adjacent

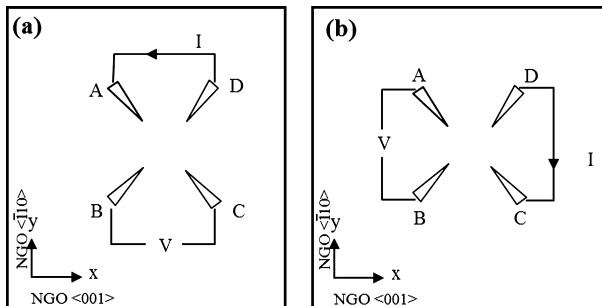


**Figure 1.** Schematic illustration of setups for a four-terminal method used in thin film electrical resistance measurement. (a) The current is applied between probes A and D, and voltage is measured between probes B and C. The nominal resistance (slope of  $V$ - $I$  curve) is obtained as  $R_x$ . (b) Current is applied between probes C and D, and voltage is measured between probes A and B. As-obtained resistance is denoted as  $R_y$ .

electrodes, and the voltage potential is measured on the other pair of electrodes by using a Keithley 4200. Thus, the nominal resistance ( $R_x$  and  $R_y$ ) can, therefore, be derived by using the traditional Van der Pauw technique.<sup>25,31</sup>

The crystalline quality of the LBCO films was characterized by the XRD  $\theta$ - $2\theta$  scan and rocking curving,  $\phi$  scan. Figure 2

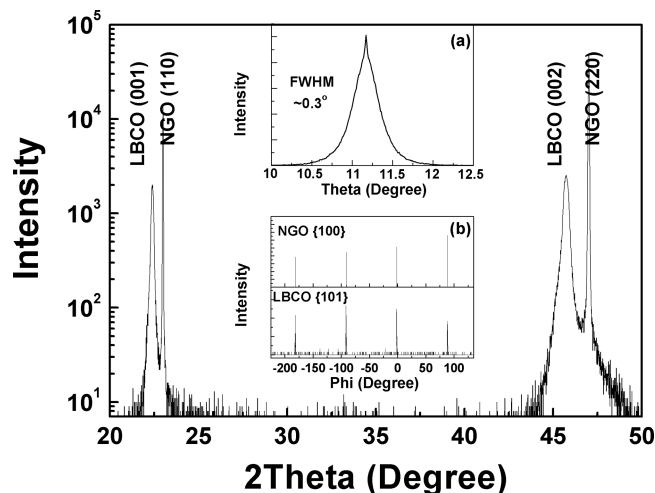


**Figure 2.** Typical XRD pattern of the LBCO films on (110) NGO substrates. The inset (a) shows the rocking curve measurement from the (001) diffraction peak of an LBCO film. The inset (b) shows the  $\phi$  scans taken around the (101) diffraction of the LBCO film.

shows a typical  $\theta$ - $2\theta$  scan for the LBCO films on (110) NGO substrates. Only the (00l) peaks appear in the  $\theta$ - $2\theta$  scans for the LBCO films, revealing that the films are oriented with the  $c$ -axis normal to the substrate surface. The rocking curve measurements from the (001) reflections for the films show that the full width at half-maximum (FWHM) is about 0.3°, as shown in the inset (a) of Figure 2, suggesting that the as-grown LBCO films are single crystalline. The  $\phi$  scan measurements have been used to understand the in-plane crystallographic relationship between the films and the substrates. The inset (b) of Figure 2 shows the  $\phi$  scans taken around the {100} reflections of the NGO substrates and the {101} reflections of the LBCO films. The 4-fold symmetry and sharp peaks in the  $\phi$  scan pattern of the LBCO films suggest that the films have good single crystallinity and an excellent epitaxial nature. On the basis of the data of the  $\phi$  scans and  $\theta$ - $2\theta$  scan, the orientation relationship between the films and the substrates is determined as  $[100]_{\text{LBCO}}//[001]_{\text{NGO}}$  and  $(001)_{\text{LBCO}}//$  (110)<sub>NGO</sub>.

The in-plane strain of the LBCO films on (110) NGO substrates has been investigated by TEM measurements of cross-sectional samples. Figure 3a shows a bright-field (BF) TEM image of a cross-sectional sample, giving an overview of the LBCO films on the (110) NGO substrate. The film–substrate interface looks sharp as denoted by a horizontal arrow. The thickness of the LBCO films is measured about 450 nm. To check the strain state of the LBCO films induced by (110) NGO substrates, selected area electron diffraction (SAED) and high-angle annular dark-field (HAADF) imaging was performed on the cross-sectional TEM samples prepared in two orthogonal directions. The SAED patterns taken along the [110] and [001] zone axes of NGO are shown in Figure 3b,c, respectively, which were obtained by using an aperture covering the LBCO films and parts of the NGO substrate. The diffraction spots with high indexes are well-separated from each other for the LBCO and NGO. For instance, the inset in Figure 3b shows the separation of the diffraction peaks between  $3\bar{3}2_{\text{NGO}}$  and  $013_{\text{LBCO}}$  and that in Figure 3c shows the separation of the diffraction peaks between  $420_{\text{NGO}}$  and  $103_{\text{LBCO}}$ . Using the diffraction spots with high indexes allows us to calculate the lattice parameters of the LBCO films with a relatively high

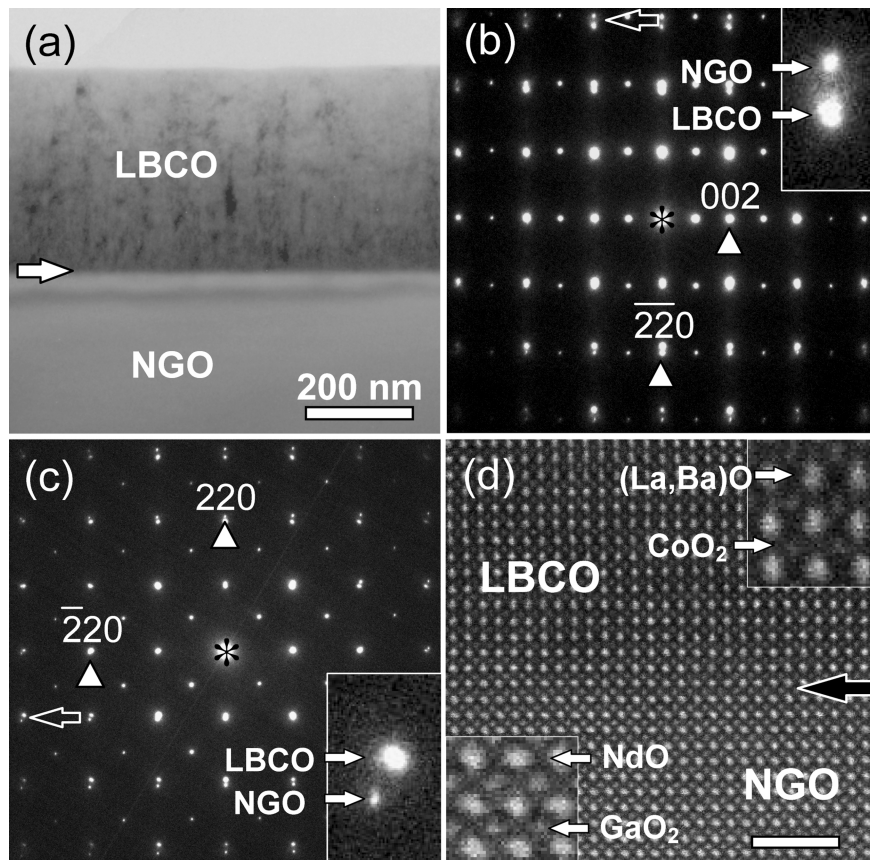


**Figure 3.** (a) A bright-field (BF) TEM image of a cross-sectional sample showing an overview of the LBCO films on the (110) NGO substrate. The film–substrate interface is denoted by a horizontal arrow. SAED pattern of the LBCO films on the NGO substrates was recorded along (b) the  $[\bar{1}10]$  and (c) the  $[001]$  zone axes of NGO, respectively. The insets in (b) and (c) display the separation of the diffraction spots of the LBCO film from the NGO substrate. (d) A typical HAADF image of the LBCO/NGO interface, recorded along the  $[001]$  zone axis of NGO. A horizontal black arrow denotes the film–substrate interface. NdO, GaO<sub>2</sub>, (La,Ba)O, and CoO<sub>2</sub> atomic planes were indicated by horizontal white arrows in the magnified parts of the NGO substrate and of the LBCO film. Scale bar: 2 nm.

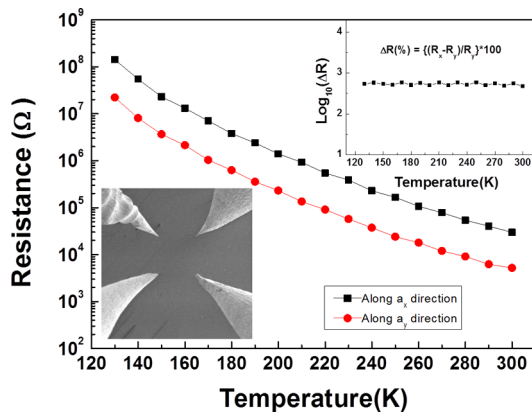
accuracy. In our calculation, the lattice parameters of the NGO substrate were used as a calibration standard. Our calculation shows that the out-of-plane parameter of LBCO is 0.397 nm. The in-plane lattice parameter of LBCO is different depending on the two orthogonal directions of  $[001]_{\text{NGO}}$  and  $[\bar{1}10]_{\text{NGO}}$ . The in-plane lattice parameter of LBCO parallel to the  $[001]_{\text{NGO}}$  is 0.386 nm and that parallel to the  $[\bar{1}10]_{\text{NGO}}$  is 0.390 nm. In comparison with LBCO bulk with a cubic structure ( $a = 3.886 \text{ \AA}$ ),<sup>18</sup> the epitaxial LBCO films exhibit orthorhombic distortion and an increased unit cell volume, resulting from the constrain of the NGO substrate. Taking the volume of the unit cell as constant, the lattice parameter of the “relaxed” cubic structure of the film is calculated as  $a_0 = 3.91 \text{ \AA}$ . Considering the lattice parameters of the NGO along the  $[001]$  and the  $[\bar{1}10]$  directions, the in-plane strain is obtained as  $(a - a_0)/a_0$  is  $-1.23\%$  along the  $[001]_{\text{NGO}}$  direction and  $-0.3\%$  along the  $[\bar{1}10]_{\text{NGO}}$  direction.

Figure 3d shows an atomic-resolution HAADF image of the interface between the LBCO film and the NGO substrate. The contrast of the HAADF image is atomic-number-dependent, and the image intensity is approximately proportional to the square of the mean atomic number  $Z$  in the columns. As a consequence, in the image of Figure 3d, the brightest dots correspond to the Nd atom columns, following by those with the decreased intensity for the La(Ba) via GaO to CoO columns. The NdO and GaO<sub>2</sub> atomic planes in NGO and

(La,Ba)O and CoO<sub>2</sub> atomic planes in LBCO are indicated by horizontal white arrows in the magnified HAADF image. In the HAADF image, oxygen atomic columns alone are not visible due to their low nuclear charge value in the LBCO/NGO system.

According to the separation of diffraction spots with high indexes in Figure 3b,c, relaxation of the in-plane strain in the LBCO films mainly occurs along the  $[\bar{1}10]$  direction of NGO. However, no misfit dislocations were observed at the film–substrate interfaces viewed along both  $[\bar{1}10]$  and  $[001]$  zone axes of the NGO substrate. The dislocation-free interfaces provide evidence for a coherent growth of the LBCO films on the (110) NGO substrates. Thus, the in-plane strain relaxation of the LBCO films along the  $[\bar{1}10]$  direction of NGO, which is measured from the SAED patterns, can be understood by lattice defects occurring within the LBCO films. Indeed, contrast variation is visible in the image locations within the LBCO film in Figure 3a. This contrast variation can be induced by various defects.

In order to investigate the possible anisotropy of in-plane electronic properties of the LBCO films, the resistance along the  $[100]$  ( $a_x$ ) direction and the  $[010]$  ( $a_y$ ) direction was measured by an ultra-high-vacuum 4P-STM system at different temperatures. Four electrodes were gold tips, fabricated by a standard chemical etching technique, to ensure good electrical contact, as shown in the bottom left inset of Figure 4. As shown



**Figure 4.** Electrical resistance of the LBCO films along the [001] direction ( $a_x$ ) and the  $[\bar{1}10]$  direction ( $a_y$ ) of the NGO substrates as a function of temperature. In the bottom left inset is the SEM image showing the four gold tips in contact with the LBCO surface. In the upper right inset is the relative difference in resistance along the two orthogonal directions as a function of temperature.

in Figure 4, it can be clearly seen that the resistance along the [010] direction is smaller than that along the [100] direction. For perovskite oxides, the properties are very sensitive to details of structural changes, due to the strong electron–lattice coupling. The strain in the films induced by the lattice mismatch will distort the  $\text{CoO}_6$  octahedra and thus change the Co–O–Co bond length and bond angle. In the double-exchange model for magnetism, the exchange energy ( $J$ ) is proportional to the electron transfer integral ( $t$ ), and the in-plane transfer integral ( $t$ ) in manganites is proportional to  $\cos(\Phi)/d^{3.5}$ , where  $\Phi$  is the in-plane bond angle and  $d$  is bond length.<sup>32,33</sup> Thus, the resistance is related to the bond length and bond angle. Compressive strain will reduce the bond length and should lead to an increase of the transfer integral and increase the hopping rate and decrease the resistance. However, the strain also changes the bond angle to deviate from  $180^\circ$  and reduces the carrier hopping and the resistance increase. In our case, the resistance measured along the [100] direction of LBCO is larger than that along the [010] direction of LBCO, which can be related to the difference in the in-plan compressive strain along the [100] form along the [010] direction of LBCO films. It is shown that resistance increases with the compressive strain. This relation is interpretable if the bond angle plays a key role in the carrier transport of LBCO thin film.

As shown in the upper right inset of Figure 4, the anisotropy in resistance,<sup>34</sup> the relative difference in resistance along the two orthogonal directions compared at the same temperature, can go up to 474% at room temperature. The maximum difference around 590% was achieved at 250 K, indicating that the anisotropic strain can significantly influence the resistivity of the film. This means that, even in the same plane, the resistance can change dramatically along different directions under anisotropic strain field.

## CONCLUSION

In summary, ferromagnetic LBCO thin films were epitaxially grown on (110)  $\text{NdGaO}_3$  substrates by pulsed laser deposition. The anisotropic in-plane strain in the LBCO thin films can be induced by using the (110)  $\text{NdGaO}_3$  substrates. Significant differences in the resistance have been measured along two orthogonal directions, [100] and [010], of the LBCO films. On

the basis of significant anisotropy in the resistance, the LBCO films possibly can be considered as potential materials for sensors for detecting subtle changes of the external strain field.

## AUTHOR INFORMATION

### Corresponding Authors

\*E-mail: m.liu@mail.xjtu.edu.cn (M.L.).

\*E-mail: cl.chen@utsa.edu (C.C.).

### Author Contributions

#These authors contributed equally to this work.

### Notes

The authors declare no competing financial interest.

## ACKNOWLEDGMENTS

This research was partially supported by the National Science Foundation under NSF-NIRT-0709293, the Natural Science Foundation of China (Nos. 51202185, 11028409, and 51390472), the Department of Energy under DE-FE0003780, and the State of Texas through the Texas Center for Superconductivity at the University of Houston.

## REFERENCES

- (1) Qi, T. F.; Korneta, O. B.; Parkin, S.; De Long, L. E.; Schlottmann, P.; Cao, G. Negative Volume Thermal Expansion Via Orbital and Magnetic Orders in  $\text{Ca}_2\text{Ru}_{1-x}\text{Cr}_x\text{O}_4$  ( $0 < x < 0.13$ ). *Phys. Rev. Lett.* **2010**, *105*, 17720.
- (2) Bao, W.; Mao, Z. Q.; Qu, Z.; Lynn, J. W. Spin Valve Effect and Magnetoresistivity in Single Crystalline  $\text{Ca}_2\text{Ru}_3\text{O}_7$ . *Phys. Rev. Lett.* **2008**, *100*, 247203.
- (3) Xiong, G. C.; Li, Q.; Ju, H. L.; Greene, R. L.; Venkatesan, T. Giant Magnetoresistance in Epitaxial  $\text{Nd}_{0.7}\text{Sr}_{0.3}\text{MnO}_{3-\delta}$  Thin-Films. *Appl. Phys. Lett.* **1995**, *66*, 1689–1691.
- (4) Jacobson, A. J. Materials for Solid Oxide Fuel Cells. *Chem. Mater.* **2010**, *22*, 660–674.
- (5) DeSouza, R. A.; Kilner, J. A. Oxygen Transport in  $\text{La}_{1-x}\text{Sr}_x\text{Mn}_{1-y}\text{Co}_y\text{O}_{3-\delta}$  Perovskites - Part I. Oxygen Tracer Diffusion. *Solid State Ionics* **1998**, *106*, 175–187.
- (6) Post, M. L.; Tunney, J. J.; Yang, D.; Du, X.; Singleton, D. L. Material Chemistry of Perovskite Compounds as Chemical Sensors. *Sens. Actuators, B* **1999**, *59*, 190–194.
- (7) Wang, D.; Tunney, J. J.; Du, X.; Singleton; Post, M. L.; Gauvin, R. Thermal Stability of  $\text{SrFeO}_3/\text{Al}_2\text{O}_3$  Thin Films: Transmission Electron Microscopy Study and Conductometric Sensing Response. *J. Appl. Phys.* **2008**, *104*, 023530.
- (8) Wang, S.; Verma, A.; Yang, Y. L.; Jacobson, A. J.; Abeles, B. The Effect of the Magnitude of the Oxygen Partial Pressure Change in Electrical Conductivity Relaxation Measurements: Oxygen Transport Kinetics in  $\text{La}_{0.5}\text{Sr}_{0.5}\text{CoO}_{3-\delta}$ . *Solid State Ionics* **2001**, *140*, 125–131.
- (9) Fauth, F.; Suard, E.; Caignaert, V. Intermediate Spin State of  $\text{Co}^{3+}$  and  $\text{Co}^{4+}$  Ions in  $\text{La}_{0.5}\text{Ba}_{0.5}\text{CoO}_3$  Evidenced by Jahn-Teller Distortions. *Phys. Rev. B* **2002**, *65*, 060401.
- (10) Luo, G. P.; Wang, Y. S.; Chen, S. Y.; Liou, Y.; Heilman, A. K.; Min, N. B.; Chen, C. L.; Chu, C. W. Electrical and Magnetic Properties of  $\text{La}_{0.5}\text{Sr}_{0.5}\text{CoO}_3$  Thin Films. *Appl. Phys. Lett.* **2000**, *76*, 1908–1910.
- (11) Taskin, A. A.; Lavrov, A. N.; Yoichi, A. Achieving Fast Oxygen Diffusion in Perovskites by Cation Ordering. *Appl. Phys. Lett.* **2005**, *86*, 091910.
- (12) Kim, G.; Wang, S.; Jacobson, A. J.; Chen, C. L.; Reimus, L.; Brodersen, P.; Mims, C. A. Oxygen Exchange Kinetics of Epitaxial  $\text{PrBaCo}_2\text{O}_{5+\delta}$  Thin Films. *Appl. Phys. Lett.* **2006**, *88*, 024103.
- (13) Kim, G.; Wang, S.; Jacobson, A. J.; Reimus, L.; Brodersen, P.; Mims, C. A. Rapid Oxygen Ion Diffusion and Surface Exchange Kinetics in  $\text{PrBaCo}_2\text{O}_{5+\delta}$  with a Perovskite Related Structure and Ordered A Cations. *J. Mater. Chem.* **2007**, *17*, 2500–2505.
- (14) Yuan, Z.; Liu, J.; Chen, C. L.; Wang, C. H.; Luo, X. G.; Chen, X. H.; Kim, G. T.; Huang, D. X.; Wang, S. S.; Jacobson, A. J.; Donner, W.

- Epitaxial Behavior and Transport Properties of  $\text{PrBaCo}_2\text{O}_5$  Thin Films on (001)  $\text{SrTiO}_3$ . *Appl. Phys. Lett.* **2007**, *90*, 212111.
- (15) Fauth, F.; Suard, E.; Caaignaert, V.; Domenges, B.; Mirebeau, L.; Keller, L. Interplay of Structural, Magnetic and Transport Properties in The Layered Co-Based Perovskite  $\text{LnBaCo}_2\text{O}_5$  ( $\text{Ln} = \text{Tb}, \text{Dy}, \text{Ho}$ ). *Eur. Phys. J. B* **2001**, *21*, 163–174.
- (16) Nakajima, T.; Ichihara, M.; Ueda, Y. New A-Site Ordered Perovskite Cobaltite  $\text{LaBaCo}_2\text{O}_6$ : Synthesis, Structure, Physical Property and Cation Order-Disorder Effect. *J. Phys. Soc. Jpn.* **2005**, *74*, 1572–1577.
- (17) Kundu, A. K.; Rautama, E.-L.; Boullay, P.; Caaignaert, V.; Pralong, V.; Raveau, B. Spin-Locking Effect in The Nanoscale Ordered Perovskite Cobaltite  $\text{LaBaCo}_2\text{O}_6$ . *Phys. Rev. B* **2007**, *76*, 184432.
- (18) Rautama, E. L.; Boullay, P.; Kundu, A. K.; Caaignaert, V.; Pralong, V.; Karppinen, M.; Raveau, B. Cationic Ordering and Microstructural Effects in the Ferromagnetic Perovskite  $\text{La}_{0.5}\text{Ba}_{0.5}\text{CoO}_3$ : Impact upon Magnetotransport Properties. *Chem. Mater.* **2008**, *20*, 2742–2750.
- (19) Rautama, E. L.; Caaignaert, V.; Boullay, P.; Kundu, A. K.; Pralong, V.; Karppinen, M.; Ritter, C.; Raveau, B. New Member of the "112" Family,  $\text{LaBaCo}_2\text{O}_{5.5}$ : Synthesis, Structure, and Magnetism. *Chem. Mater.* **2009**, *21*, 102–109.
- (20) Liu, J.; Liu, M.; Collins, G.; Chen, C. L.; Jiang, X. J.; Gong, W. Q.; Jacobson, A. J.; He, J.; Jiang, J. C.; Meletis, E. I. Epitaxial Nature and Transport Properties in  $(\text{LaBa})\text{Co}_2\text{O}_{5+\delta}$  Thin Films. *Chem. Mater.* **2010**, *22*, 799–802.
- (21) Liu, J.; Collins, G.; Liu, M.; Chen, C. L.; Jiang, J. C.; Meletis, E. I.; Zhang, Q. Y.; Dong, C. PO<sub>2</sub> Dependant Resistance Switch Effect in Highly Epitaxial  $(\text{LaBa})\text{Co}_2\text{O}_{5+\delta}$  Thin Films. *Appl. Phys. Lett.* **2010**, *97*, 094101.
- (22) Liu, M.; Liu, J.; Collins, G.; Ma, C. R.; Chen, C. L.; He, J.; Jiang, J. C.; Meletis, E. I.; Jacobson, A. J.; Zhang, Q. Y. Magnetic and Transport Properties of Epitaxial  $(\text{LaBa})\text{Co}_2\text{O}_{5.5+\delta}$  Thin Films on (001)  $\text{SrTiO}_3$ . *Appl. Phys. Lett.* **2010**, *96*, 132106.
- (23) Ma, C. R.; Liu, M.; Collins, G.; Wang, H. B.; Bao, S. Y.; Xu, X.; Enriquez, E.; Chen, C. L.; Lin, Y.; Whangbo, M. H. Magnetic and Electrical Transport Properties of  $\text{LaBaCo}_2\text{O}_{5.5+\delta}$  Thin Films on Vicinal (001)  $\text{SrTiO}_3$  Surfaces. *ACS Appl. Mater. Interfaces* **2013**, *5*, 451–455.
- (24) Liu, M.; Ma, C. R.; Liu, J.; Collins, G.; Chen, C. L.; He, J.; Jiang, J. C.; Meletis, E. I.; Sun, L.; Jacobson, A. J.; Whangbo, M. H. Giant Magnetoresistance and Anomalous Magnetic Properties of Highly Epitaxial Ferromagnetic  $(\text{LaBa})\text{Co}_2\text{O}_{5.5+\delta}$  Thin Films on (001)  $\text{MgO}$ . *ACS Appl. Mater. Interfaces* **2012**, *4*, 5524–5528.
- (25) Lu, H. L.; Zhang, C. D.; Guo, H. M.; Gao, H. J.; Liu, M.; Liu, J. A.; Collins, G.; Chen, C. L. Surface-Step-Terrace-Induced Anomalous Transport Properties in Highly Epitaxial  $\text{La}_{0.67}\text{Ca}_{0.33}\text{MnO}_3$  Thin Films. *ACS Appl. Mater. Interfaces* **2010**, *2*, 2496–2499.
- (26) Ma, C. R.; Liu, M.; Liu, J.; Collins, G.; Zhang, Y. M.; Wang, H. B.; Chen, C. L.; Lin, Y.; He, J.; Jiang, J. C.; Meletis, E. I.; Jacobson, A. J. Interface Effects on the Electronic Transport Properties in Highly Epitaxial  $\text{LaBaCo}_2\text{O}_{5.5+\delta}$  Films. *ACS Appl. Mater. Interfaces* **2014**, *6*, 2540–2545.
- (27) Lin, Y.; Chen, X.; Liu, X. W.; Chen, C. L.; Lee, J. S.; Li, Y.; Jia, Q. X.; Bhalla, A. Epitaxial Nature and Anisotropic Dielectric Properties of  $(\text{Pb},\text{Sr})\text{TiO}_3$  Thin Films on  $\text{NdGaO}_3$  Substrates. *Appl. Phys. Lett.* **2005**, *86*, 142902.
- (28) Lin, Y.; Chen, X.; Liu, X. W.; Chen, C. L.; Lee, J. S.; Li, Y.; Jia, Q. X.; Bhalla, A. Anisotropic In-Plane Strains and Dielectric Properties in  $(\text{Pb},\text{Sr})\text{TiO}_3$  Thin Films on  $\text{NdGaO}_3$  Substrates. *Appl. Phys. Lett.* **2004**, *84*, 577–579.
- (29) Huang, Z.; Wang, L. F.; Chen, P. F.; Gao, G. Y.; Tan, X. L.; Zhi, B. W.; Xuan, X. F.; Wu, W. B. Tuning the Ground State of  $\text{La}_{0.67}\text{Ca}_{0.33}\text{MnO}_3$  Films via Coherent Growth on Orthorhombic  $\text{NdGaO}_3$  Substrates with Different Orientations. *Phys. Rev. B* **2012**, *82*, 014410.
- (30) Schmidbauer, M.; Kwasniewski, A.; Schwarzkopf, J. High-Precision Absolute Lattice Parameter Determination of  $\text{SrTiO}_3$ ,  $\text{DyScO}_3$  and  $\text{NdGaO}_3$  Single Crystals. *Acta Crystallogr., Sect. B: Struct. Sci.* **2012**, *68*, 8–14.
- (31) Zou, Q.; Liu, M.; Wang, G. Q.; Lu, H. L.; Yang, T. Z.; Guo, H. M.; Ma, C. R.; Xu, X.; Zhang, M. H.; Jiang, J. C.; Meletis, E. I.; Lin, Y.; Gao, H. J. Step Terrace Tuned Anisotropic Transport Properties of Highly Epitaxial  $\text{LaBaCo}_2\text{O}_{5.5+\delta}$  Thin Films on Vicinal  $\text{SrTiO}_3$  Substrates. *ACS Appl. Mater. Interfaces* **2014**, *6*, 6704–6708.
- (32) Xie, C. K.; Budnick, J. I.; Hines, W. A.; Wells, B. O.; Woicik, J. C. Strain-Induced Change in Local Structure and Its Effect on The Ferromagnetic Properties of  $\text{La}_{0.5}\text{Sr}_{0.5}\text{CoO}_3$  Thin Films. *Appl. Phys. Lett.* **2008**, *93*, 182507.
- (33) Xiong, Y. M.; Wang, G. Y.; Luo, X. G.; Wang, C. H.; Chen, X. H.; Chen, X.; Chen, C. L. Magnetotransport Properties in  $\text{La}_{1-x}\text{Ca}_x\text{MnO}_3$  ( $x = 0.33, 0.5$ ) Thin Films Deposited on Different Substrates. *J. Appl. Phys.* **2005**, *97*, 083909.
- (34) Ward, T. Z.; Budai, J. D.; Gai, Z.; Tischler, J. Z.; Yin, L. F.; Shen, J. Elastically Driven Anisotropic Percolation in Electronic Phase-Separated Manganites. *Nat. Phys.* **2009**, *5*, 885–888.